Egyptian Journal of Chemistry

http://ejchem.journals.ekb.eg/

Effect of The Precursors and Synthesis Methods on The Optical and Photo- electrochemical Characteristics of SnS Absorber Layer

Atef Y. Shenouda[1*], M.M.S. Sanad[1] and Ofeliya Kostadinova[2]

[1]Central Metallurgical Research and Development Institute (CMRDI), Tebbin, P.O. Box 87 Helwan, Egypt.
[2]Institute of Electrochemistry and Energy Systems (IEES), Bulgarian Academy of Sciences, 10 Acad. G. Bonchev Bl. 10, 1113 Sofia, Bulgaria.

INFLUENCE of the preparation method and different precursors are important for the absorber photovoltaic layer parameters of SnS. Synthesis of SnS compounds was carried out via two preparation methods; solid state reaction and hydrothermal; using different sulfur precursors. The morphology of particles and phase identification were studied using Field Emission Scanning Electron Microscope (FESEM) and X-ray diffraction (XRD) techniques. The XRD diffraction pattern of SnS revealed the existence of two crystal structure phases: the major is orthorhombic and the minor phase is tetragonal. The optical properties were determined using UV-Vis spectrophotometer showing absorbance peaks around 485 nm. The lowest bandgap of 1.74 eV is for SnS sample prepared from L-cystine. Electrochemical impedance spectroscopy (EIS) revealed that SnS cell prepared from L-cystine gave the lowest resistance of 171Ω. The photoelectrochemical measurements of this cell showed the highest power conversion efficiency per unit area of 2.5%.

Keywords: SnS absorber layer, Electrochemical impedance spectroscopy, Photoelectrochemical investigation.

Introduction

Among various renewable energy precursors developing nowadays, solar cells have the greatest potential to provide clean and safe power since their "fuel" is abundant, limitless and clean that is solar light. The solar cell components include a semiconductor layer that absorbs part of the light. Thus, it generates charge carriers and then separates them. Therefore, such layer can be considered as one of the most important part of a solar cell. Good absorber material has to be a semiconductor with an absorption coefficient of 10^5 cm^{-1}, a bandgap of ~1.5 eV, high quantum efficiency of excited carriers, long diffusion length and low recombination velocity. Besides, the constituent materials must be abundant, cheap and non-toxic [1-3].

In this regard, Tin (II) sulphide (SnS) is

considered as a good and promising candidate. It has a direct band gap semiconductor compound. Also, it has recently received great attention due to its unique properties during the last years [4]. This is due to its suitable optical and electrical properties to be applied as an absorbent material for thin film photovoltaic cell. Because of low cost, absence of toxicity and good abundance in nature, it becomes a candidate for future multifunctional devices particularly for light conversion applications. Although the current efficiencies are low, the cost-per-Watt is becoming attractive and competitive. Also, it has other applications such as lithium batteries.

SnS characteristics are highly affected by the preparation method. Clearly, SnS is a p-type semiconductor with either tetragonal or orthorhombic unit cell depending on synthesis method [4]. It was reported that preparation

method determines also important parameters like band gap width.

SnS has direct 1.2–1.5 eV [5,6] and indirect optical band gap of 1–1.2 eV [7, 8]. It has a high absorption coefficient, conductivity, α more than 10^4 cm^{-1}[9], a high carrier concentration and mobility (hole mobility ~ 90 cm^2 V^{-1} s^{-1}) that have made it a promising candidate for photovoltaic [2,10,11], photoelectrochemical cell [12,13], Li ion battery anodes [14], electrochemical capacitors [15] and photodetectors [16].

The crystal structure and lattice parameters were studied at normal temperature and pressure (NTP) [4]. The SnS compound usually possesses orthorhombic disorder crystal-structure with a space group $\left(\mathbf{D}_{2h}^{16} = \mathbf{Pcmn}\right)$ of having a=0.432, b=1.12 and c=0.398 nm (JCPDS card No: 39-0354) as lattice parameters. Also, it was reported that the synthesis at room temperature, SnS found a stable low symmetric, double-layered orthorhombic crystal structure, having a=3.978, b=4.328, and c= 11.193 Å, as lattice parameters [17]. Above 875 K, SnS undergoes an orthorhombic-to-tetragonal phase transition. The lattice parameters of the high-temperature phase are: a= 4.23 Å and c= 11.51 Å.

Influence of synthesis parameters was extensively studied in the work of Robles et.al. [18], where tin sulfide thin films were prepared by co-evaporation at operating temperatures ranging from 200 to 400°C. The structural, chemical, optical and electrical properties were found to be strongly dependent on substrate annealing conditions.

Therefore, the aim of this work is to prepare pure SnS materials using two different methods, solid state reaction (SSR) in case of elemental S and different raw-materials as S-precursors in the hydrothermal reaction (HTR). In addition, sufficient comparative studies are conducted to investigate the optimum structures and physicochemical properties that could lead to increase in: (i) absorbance of sun-light, (ii) active surface area, (iii) electrical conductivity and (iv) solar cell conversion efficiency.

Experimental

Synthesis of SnS from different precursors of Sulphur (S).

Different samples of SnS were prepared following hydrothermal approach by using the stoichiometric ratios of SnCl$_2$.2H$_2$O and one of

the initial materials, Na$_2$S.9H$_2$O, thio-acetamide (TAM), thiourea (TU), thio-acetic acid (TAA) and L-cystine. The precursors were dissolved separately in small amount of distilled water, mixed with SnCl$_2$.2H$_2$O and heated at 100°C for 6 h under stirring. This solution was treated hydrothermaly in a Teflon Vessel with stainless steel cover autoclave of volume 250 cm^3 at 200 °C for 24 hours. The prepared black precipitate of each sample was filtered off, washed with distilled water and ethanol and then dried in an oven at 60°C for 6 h. The powders and also SnS prepared from elements powders (Sn and S) using SSR method were mixed and ground. After that, they were transferred into a crucible boat, heated at 500°C under argon with 5 % H$_2$ atmosphere in a tube furnace, kept for 8 hours and cooled down to room temperature.

Characterizationand measurements.

The dried powder was investigated by XRD on a Brucker axis D8 diffractometer with crystallographic data software Topas 2 using Cu-Kα (λ= 1.5406 nm) radiation, operating at 40 kV and 30mA. The angle scan rate was set at 2°/min.The microstructure and morphology of the samples were characterized by Field emission electron microscope (FE-SEM QUANTAFEG 250).

The optical measurements were performed using UV–Vis–NIR Spectrophotometer (Perkin Elmer lambda 1050 Spectrophotometer, USA). The electrochemical impedance spectra (EIS) and photoelectrochemical cell measurements were carried out with SnS coated on conducting indium tin oxide (ITO) glass substrate (SPI Company, USA). The coated area was 2.5 cm x 4 cm. The signal amplitude was 10 mV and the frequency range was 10^6 Hz -10 mHz. EIS measurements were carried out using PARASTAT 4000 (Princeton, USA). The photoelectrochemical cell configuration was set up as: Glass/ITO/ SnS/ 0.5 M KI + 0.5 M I$_2$ + 0.5 M NaOH/C (graphite). Xenon arc lamp 150 W was applied as a light source with solar simulator Sciencetech SS150W-AAA. The cell was exposed to light intensity 1 Sun (100 mW/cm^2) using Air Mass 1.5 Global Filter. A 2400 Keithley Source Meter SSIVT-60WC was used as I-V meter. The calibrated reference cell consists of a 20 x 20 mm monocrystalline silicon (model SC-LT) photovoltaic cell encased in a 92 x 70 x 16 mm metal enclosure with a protective quartz window. The reference detector (SSIVT-refl) effective in sensing wavelengths between

190 nm and 1100 nm is calibrated with the 1 sun. Parameters measured by IV Software program were V_{oc}, I_{sc}, P_{max}, R_{series}, R_{shunt} and FF (where: V_{oc} stands for open circuit potential of the working electrode, I_{sc} denotes short circuit current measured at zero voltage, $P_{max} = V_{max} \times I_{max}$, V_{max}, and I_{max} are the maximum voltage and current of the I-V relation, R_{series}: series resistance, R_{shunt}: shunt resistance, FF: filling factor).

Results and Discussion

Material characterization

The prepared SnS samples from different precursors of S were characterized after annealing by XRD as shown in Fig.1. The peaks of SnS reveal the existence of two crystal structure phases: one phase is a tetragonal [14], which is minor at 14.56° (110) & 21.6° (202) and the other major one is orthorhombic [11, 15, 16] at 16.12° (004), 26.09° (201) , 27.35° (210), 30.5° (101), 31.55 (111), 39° (311), 42.46° (210), 44.9° (411), 45.4° (002) and 48.28° (211), 51.3° (121), 66.24° (800). The sample prepared by hydrothermal reaction (HR) shows wider diffraction peaks rather than the sample obtained using solid-state reaction from elemental sources. This is due to the lower particle and crystallite sizes of samples prepared by HR.

The crystallite size *"L"* of the samples was calculated using the X-ray line width, **β** at full width half maximum (FWHM) according to the Scherer formula [19, 20]:

$$L = 0.94 \, \lambda/\beta \cos \theta \qquad (1)$$

Where; L is the crystallite size, λ is wavelength of the target (0.15406 nm for Cu) and θ is the chosen diffraction angle [14]. Using 2θ equals to 32.16° for SnS, the crystallite sizes for all samples are calculated and the values are presented in Table 1. The lowest value of 35.6 nm is obtained for the sample prepared from using L-Cystine.

SEM characterization

The influence of the preparation method, and the S-precursors, respectively, on the morphology of the obtained materials was assessed with the aid of FESEM. It is revealed that solid state reaction from elements provides oblong oval particles with average size of 1μm. Moreover, tiny and rectangular-like shape is observed for materials produced by Na₂S and has sub-micron particle size. Furthermore, the platelet-like morphology is obtained for using TAM as S-source. The fused,

high dense and flattened particles are revealed for sulphide material prepared from TAA. Finally, the SnS sample prepared from L-cystine displayed a flower-like structure as shown in Fig. 2. The comparison between the two routes applied (solid state and hydrothermal reactions) for SnS formation showed that higher grain sizes and roughness were obtained by sulfurization of metallic precursors rather than crystal growth of the SnS prepared by hydrothermal reaction at T=200°C.

Optical spectra and electrical measurements

Optical characteristics of the material, such as high absorption coefficient and optical energy band gab are of a crucial importance for its potential application in the solar cell. Therefore, the optical spectra of the six samples were measured using the spectrophotometer and the results are shown in Fig. 3. All samples show highest absorbance around 485 nm. The absorption of the sample prepared from TAM is the weakest, represented by a tiny single peak, while all other samples display a peak with higher intensity widen by a shoulder that is located at 446 nm.

The absorption coefficient "α", a very important parameter for an absorber material is given by the following relations [21-23]:

$$\text{Log} \, (1 / T) = \alpha \, t \qquad (2)$$

$$\text{The absorbance A} = \text{Log} \, (I° /I) = \alpha \, t \qquad (3)$$

$$\text{Transmittance \% T} = 100 \, (I / I°) \qquad (4)$$

where; T is the transmittance of the spectra, t is the film thickness and I and I° are the intensities of the incident and transmitted light through the sample. From these spectral data, the absorption coefficient (α) for direct electron transition semiconductors is given by [21-23]:

$$\alpha h = A \, (h-E_g)^{0.5} \qquad (5)$$

E_g is the optical band gap or energy gap, A is a constant, h is Plank`s constant, ν is the frequency of the incident radiation or light (ν= c/λ; where c is the velocity of sun light and λ is the wavelength of the incident light). The absorbance coefficients of the samples are calculated and their values are given in Table 1. In general, the absorption coefficients of the samples are more than 10^4 cm^{-1}. The highest coefficient, 8.78×10^4 cm^{-1} is obtained when using L-cystine as an initial S-material, which is near to 10^5 cm^{-1}.
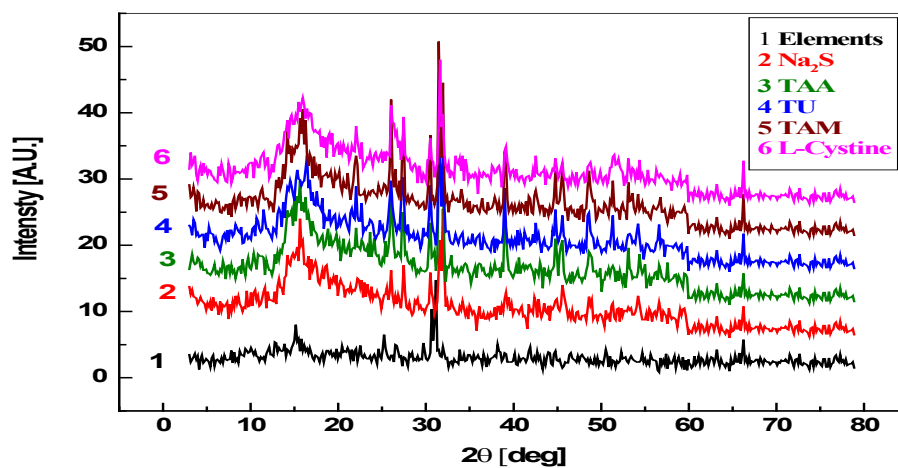
Fig. 1. X-ray diffractograms of SnS prepared from different Sulfur precursors.
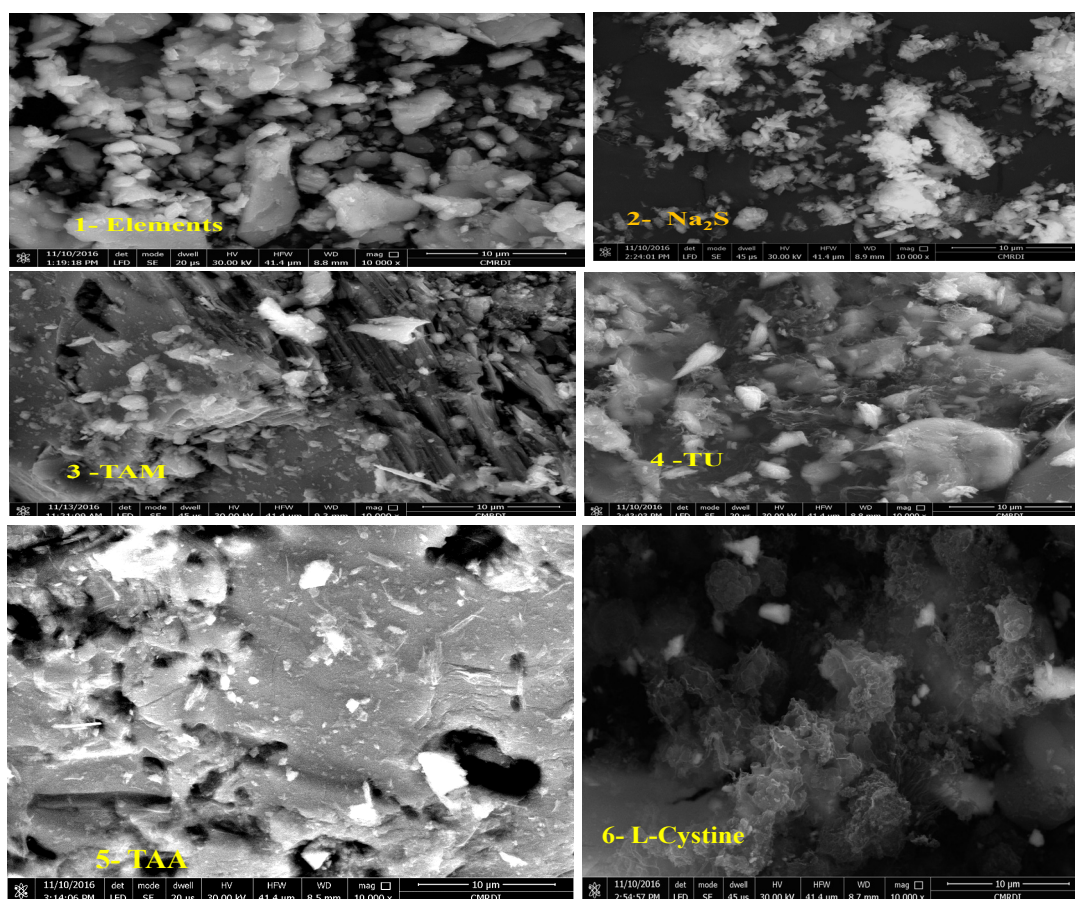

**Fig. 2 FESEM of SnS samples prepared from different Sulfur precursors, (1)
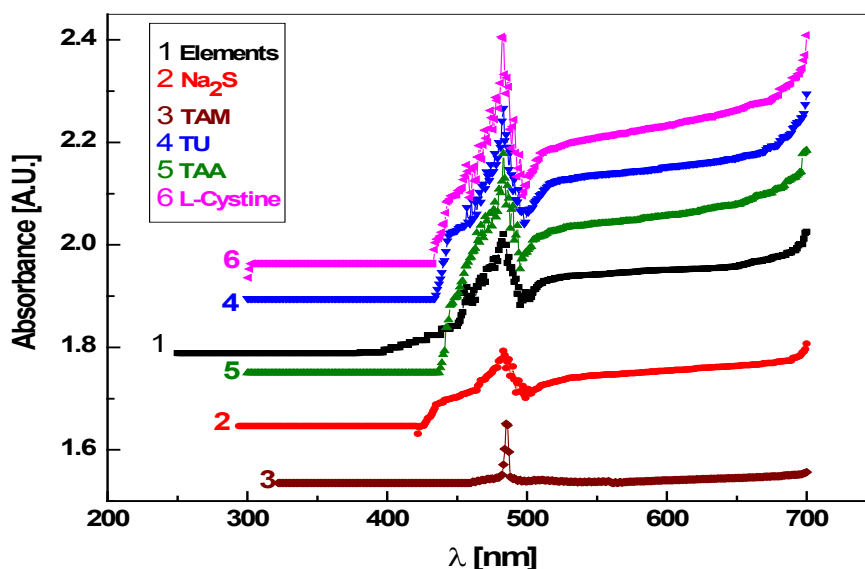elements, (2) Na₂S, (3) TAM, (4) TU, (5) TAA and (6) L-cystine .**

Fig. 3   Optical absorbance spectra of SnS prepared from different sulfur precursors.

TABLE 1. The calculated crystallite size "*L*" using the X-ray at 2q = 32.16° after heat treatment, optical and EIS parameters of SnS samples prepared from different sulfur precursors.

Compound	L [nm]	absorption coefficient, α x 10^4 cm^{-1}	Optical band gap, eV	Cell charge transfer resistance [R_{ct}], Ω	Double layer capacitance [C_{dl}], F
L-Cyst.	35.62	8.78	1.74	171	5.94E-05
TAA	57.31	8.18	1.79	177	5.63E-05
TU	71.72	7.75	1.81	187	3.70E-05
TAM	79.22	7.32	1.85	296	1.73E-06
Na$_2$S	88.13	6.48	1.88	448	1.69E-06
Elements	117.11	5.66	1.95	847	1.42E-06

Analysis of optical absorption spectra is important for determining the optical band gap of the film. The value of the latter defines the light absorption ability in a specific wave length region.The relation between the energy gap, hν and the absorbance coefficient energy, (αhν)^2 is demonstrated in Fig. 4. The energy gap is determined by extrapolation of the curve down to x-axis and the values are presented in the Table 1. The highest value is obtained for sample prepared by elements (1.95eV), while the lowest one is achieved for L-cystine SnS (1.74eV), suggesting the latter would be the most appropriate choice for achieving higher power conversion efficiency.

The electrochemical impedance spectroscopy (EIS) is a powerful technique that is able to detect different underlying chemical processes such as charge transfer, mass transport, phase transitions [24]. This method is often applied to investigate the resistance of a material. The photo-electrochemical impedance behavior of SnS prepared from different precursors of S is depicted in Fig.5. It is observed that SnS cell prepared from L-Cystine has the lowest resistance value, 171 Ω compared to the cells prepared from other S-precursors. The charge transfer resistance, R_{ct} and the double layer capacitance, C_{dl} for all samples are represented in Table 1.
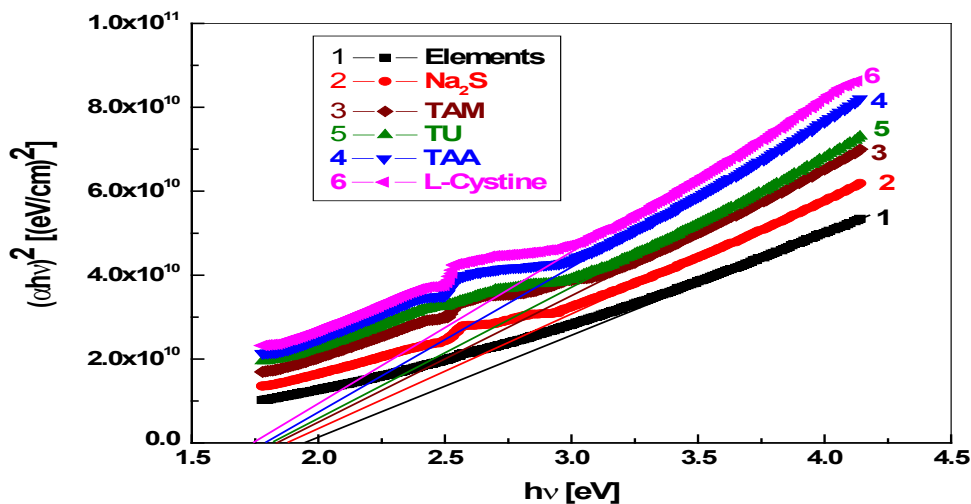
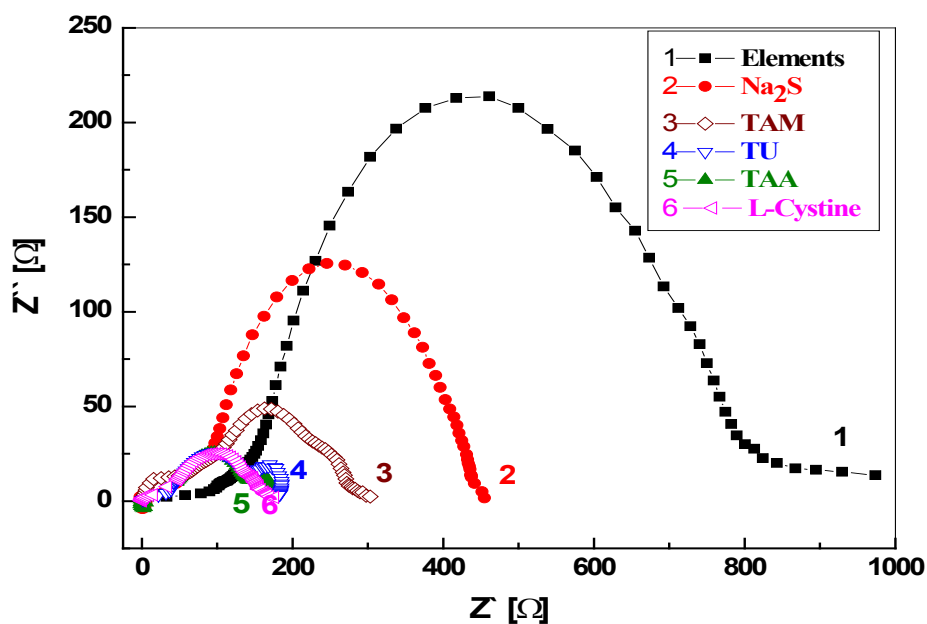**Fig. 4 Dependence of (αhν)² photon energy on hν for SnS prepared from different Sulfur precursors.**

Fig. 5 EIS of photoelectrochemical cells for SnS prepared from different Sulfur precursors.

It is observed that the lowest charge transfer resistance R_{ct}, highest conductivity and the highest C_{dl} are achieved for SnS prepared from L-cystine. It can be explained by the smallest grain size and highest surface area, which provide large mobility of charge carriers. To obtain the power output characteristics of the photo electrochemical cell

(PEC), V_{oc} and I_{sc} are recorded for the prepared CTS samples. I–V curves are illustrated in Fig. 6. The power conversion efficiency (α %) and fill factor (FF %), measures of device performance are given by the following equations [24]:

$$FF = (V_{max} \cdot I_{max} / V_{oc} \cdot I_{sc}) \cdot 100 \qquad (6)$$

$$h = (V_{max} . I_{max} / P_{in} . A) . 100 \qquad (7)$$

where: A = 10 cm^2 denotes area of the working electrode, and P_{in} is the incident intensity of the light (100 mW cm^{-2}=1Sun). The achieved solar cell parameters and efficiencies are given in Table 2. It is noticed that the photoelectrochemical SnS cell prepared from L-cystine has the highest power efficiency of 2.5% in comparison with the other cells. The high power efficiency of SnS prepared from L-cystine is attributed to the great conductivity, 1.6x10^{-6} Scm^{-1} (Table 1), which promoted by the largest mobility of charge carriers as discussed in the electrochemical impedance spectra measurements. Besides, the lower energy gap, 1.74 eV of this compound enhances the transition of the electron- hole pairs between the valence and conduction bands.

Energy band diagrams for the photoelectrochemical cell of SnS prepared from L-cystine is shown in Fig. 7. It was reported that SnS semiconductor is p-type [5, 25-28]. The graphite has energy band gap 0.04 eV [29]. The absorption of photons generates excited electronic states in illuminated semiconductor system such as SnS. These excited states have lifetimes of limited duration. Without the charge separation, their intrinsic energy would be lost through relaxation (recombination) as explained in equations 8 &9.
Light absorption

$$h\nu + SnS \longrightarrow h+_{SnS} + e-_{SnS} \qquad (8)$$

Recombination

$$h^+_{SnS} + e^-_{SnS} \longrightarrow heat \qquad (9)$$
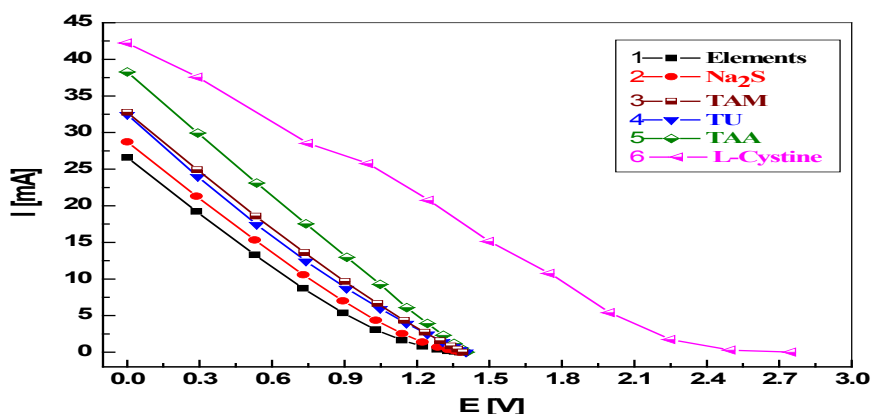
The mechanism of charge separation

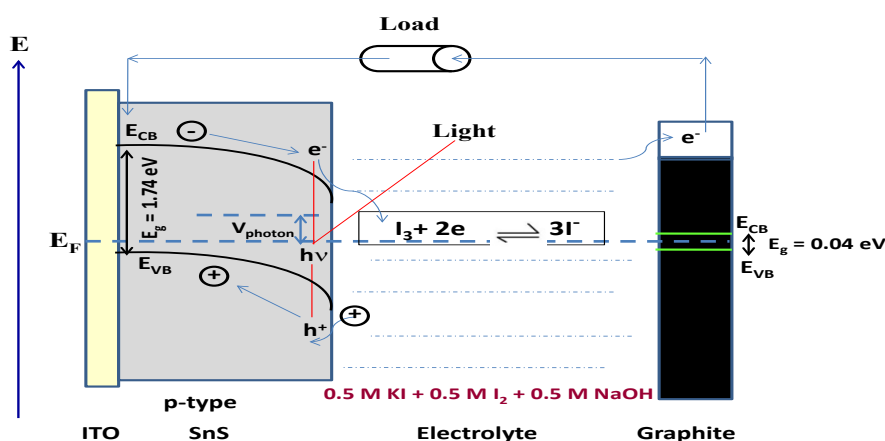**Fig. 6 Power output plot of the Photo Electrochemical cells of SnS prepared from different Sulfur precursors..**

Fig. 7 Schematic illustration of band bending for p-type SnS (from L–cystine) semiconductor inside the photoelectrochemical cell.

TABLE 2 . Photo electrochemical cells (PEC) parameters of SnS prepared from different S-sources.
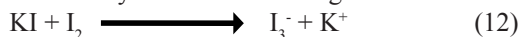
Type of cell preparation	V_{oc} [V]	I_{sc} [A]	P_{max}[W]	R_{series} [Ω]	R_{shunt} [Ω]	FF[%]	h[%]
Elements	1.37	2.66E-02	7.03E-03	63.84	39.52	19.29	0.70
Na$_2$S	1.38	2.87E-02	8.09E-03	58.02	35.33	20.42	0.80
TU	1.39	3.25E-02	9.55E-03	52.10	35.31	21.14	0.95
TAM	1.40	3.27E-02	9.94E-03	46.31	37.36	21.66	0.99
TAA	1.40	3.83E-02	1.30E-02	41.26	38.96	24.17	1.31
L-cystine	2.72	4.24E-02	2.50E-02	35.23	40.12	21.63	2.51

has been considered in designing efficient photoelectrochemical systems. At illuminated semiconductor/liquid interfaces, an electric field (the space charge layer) occurs concurrent with charge/ion redistribution at the interface. Upon photogeneration of electron/hole pairs, this electric field impedes recombinative processes by oppositely accelerating and separating these charges, resulting in minority carrier injection into the electrolytic redox couple as explained by equations 10&11.

Charge separation

$$e^-_{SnS} \longrightarrow e^-_{bulk} \qquad (10)$$
$$h^+_{SnS} \longrightarrow h^+_{surf} \qquad (11)$$
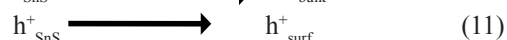
The electrolyte has the following ions:
$$KI + I_2 \longrightarrow I_3^- + K^+ \qquad (12)$$

This concept of carrier generation is illustrated in Fig. 7 for p-type SnS PEC with graphite as counter electrode is the theoretical basis for several efficient SnS semiconductor / I_3^- /3I$^-$ redox couple PEC as revealed by the interfacial reactions in equations 13&14.

Interfacial reactions

$$2e^-_{surf}+I_3^-(Ox) \longrightarrow 3I^- \quad (Red) \qquad (13)$$

$$2h^+_{surf}+3I^-(Red) \longrightarrow I_3^- \quad (Ox) \qquad (14)$$

Conclusion

SnS was synthesized by different routes: (i) direct solid state reaction from elementary Sn and S; (ii) hydrothermal reaction using different precursors of S, like Na$_2$S, TU, TAA, TAM and L-cystine.The XRD analysis showed that SnS with tetragonal symmetry is obtained in all cases. The SEM investigation showed that the preparation

method affect the morphology to a great extent. Thus, using solid state reaction from elements delivers mostly ellipsoidal particles, while SnS prepared from L-cystine has flower-like shape. The optical study reveals that the maximum of the optical absorbance of the SnS samples occurred at about 485 nm. The lowest band gap was observed for the sample, prepared from L-cystine as a sulfur – precursors. The comparison between the two routes applied for SnS formation showed that higher grain sizes and roughness were obtained by sulfurization of metallic Sn rather than crystal growth of the ones prepared by hydrothermal reaction at T=200°C. The crystalline SnS phase obtained by both methods exhibited band gap energy of about 1.72-1.95 eV, absorption coefficient (α) > 10^4 cm^{-1}. The highest coefficient, 8.78 x 10^4 cm^{-1} is obtained when using L-cystine as an initial S-material, which is near to 10^5 cm^{-1}. The electrical conductivity of is about 1.6x10^{-6} Scm^{-1}. The L-cystine sample showed the lowest resistance value and the highest conversion efficiency per unit area, 2.5%. The properties of the prepared materials can fulfill all the basic requirements for efficient absorber layer in a photovoltaic cell.

References

1. Ogah O.E., Zoppi G., Forbes I., and Miles R.W., Thermally evaporated thin films of SnS for application in solar cell devices, *Thin Solid Films*, **517**, 2485- 2488 (2009).

2. Reddy K.T.R., Reddy N. K., and Miles R.W., Photovoltaic properties of SnS based solar cells, *Sol. Ener. Mater. & Sol. Cells*, **90**, 3041- 3046 (2006).

3. Patel M., Mukhopadhyay I. and Ray A., Molar optimization of spray pyrolyzed SnS thin films for photoelectrochemical applications, *J. Alloys & Compds.* **619**, 458–463 (2015).

4. Reddy N. K., Devika M., and Gopal E. S. R., Review on Tin (II) Sulfide (SnS) Material: Synthesis, Properties, and Applications, *Critical Reviews in Solid State and Materials Sciences*, **0**, 1–40, (2015).

5. Calixto-Rodriguez M., Martinez H., Sanchez-Juarez A., Campos-Alvarez J., and Tiburcio-Silver A., Structural, optical, and electrical properties of tin sulfide thin films grown by spray pyrolysis, *Thin Solid Films*, **517,** 2497–2499 (2009).

6. Kois J., Bereznev S., Maricheva J., and Revathi N., Electrochemical and photoelectrochemical characterization of SnS photoabsorber films , *Mater. Sci. Semicond. Process.*, **58**, 76–81(2017).

7. Burton L.A., Colombara D., Abellon R.D., Grozema F.C., Peter L.M., Savenije T.J., Dennler G., and Walsh A., Synthesis, Characterization and Electronic Structure of Single Crystal SnS, Sn_2S_3, and SnS2, *Chem. Mater.*, **25**, 4908–4916 (2013).

8. Hartman K., Johnson J.L., Bertoni M.I., Recht D., Aziz M.J., Scarpulla M.A., and Buonassisi T., SnS thin-films by RF sputtering at room temperature, *Thin Solid Films*, **519**, 7421- 7424 (2011).

9. Tanusevski A., Optical and photoelectric properties of SnS thin films prepared by chemical bath deposition, *Semicond. Sci. Technol.*, **18**, 501–505 (2003).

10. Devika M., Reddy K.T.R., Reddy N.K., Ramesh K., Ganesan R., Gopal E.S.R., and Gunasekhar K.R., Microstructure dependent physical properties of evaporated tin sulfide films, *J. Appl. Phys.*, **100**, 023518-7 (2006).

11. Vidal J., Lany S., Francis J., Kokenyesi R., and Tate J., Structural and electronic modification of photovoltaic SnS by alloying, *J. Phys. Chem.*, **115**, 113507 (2014).

12. Huang P., Huang J., Wang S., Shaikh M.O., and Lin C., Photoelectrochemical properties of orthorhombic and metastable phase SnS nanocrystals synthesized by a facile colloidal method, *Thin Solid Films*, **596**, 135–139 (2015).

13. Subramanian C., Sanjeeviraja M., and Jayachandran, Cathodic electrodeposition and analysis of SnS films for photoelectrochemical cells, *Mater. Chem., Phys.,* **71**, 40–46 (2001).

14. Tian H., Xin F., Wang X., He W., and Han W., High capacity group-IV elements (Si, Ge,Sn) based anode for lithium-ion batteries, *J. Mater.*, **1,** 153–169 (2015).

15. Jayalakshmi M., Rao M. M., and Choudary B.M., Identifying nano SnS as a new electrode material for electrochemical capacitors in aqueous solutions, *Electrochem. Commun.*, **6,** 1119–1122 (2004).

16. Koppens F.H.L., Photodetectors based on graphene, other two-dimensional materials and hybrid systems, *Nat. Nanotech*, **9,** 780–793 (2014).

17. Nasirov V. I. and Adgezalova Kh. A., Stabilization of Low-Temperature SnS by Rare-Earth Doping, *Inorg. Mater.,* **37**, 1099–1100 (2001).

18. Robles V., Trigo J.F., Guillen C. and J. Herrero , Growth of SnS thin films by co-evaporation and sulfurization for useas absorber layers in solar cells, *Mater. Chem. Phys.* **167**, 165-170 (2015).

19. Badawy, A. A., Rashad, A. M., and Yehia, N. S., Physicochemical and Catalytic Conversion of Iso-propanol over NiO-doping/nanosized ZnO-Fe2 O3 system, *Egypt. J. Chem.*, **60**, 619 - 625 (2017).

20. Selim M.M., Hassan S.A., Rezk M.R.A. and Deraz N. M., Preparation and Characterization of Nano Cu and CuO Catalysts Supported on Washcoated Cordierite, *Egypt. J. Chem.*, **53**, 497-514 (2010).

21. Eraky M.S., Shenouda A.Y., Ibrahim I.A. and El-Shereafy E.E., Synthesis, characterization and performance of Cu_2SnS_3 for solar cell application, *Inter. J. Sci. & Eng. Res.*, **6**, 1447-1453 (2015).

22. Shenouda A.Y., Rashad M. M. and Chow L., Synthesis, characterization and performance of $Cd_{1-x}In_xTe$ compound for solar cell applications, *J. Alloy. & Compd*, **563**, 39–43 (2013).

23. Sanad M.M.S., Rashad M.M. and Shenouda

A.Y., Novel CuIn1-*x*Ga*x*Te₂ structures for high efficiency photo-electrochemical solarcells, *Inter. J. Electroch. Sci.*, **11**, 4337–4351 (2016).

24. Sanad M.M.S., Shalan A.E., Rashad M.M., and Mahmoud M.H.H., Plasmonic enhancement of low cost mesoporous Fe₂O₃-TiO₂ loaded with palladium, platinum or silver for dye sensitized solar cells (DSSCs), *Appl. Surf. Sci.,* **359,** 315-322 (2015).

25. Saad M. A., Nasr M. F., Yassen H. A., and Turky G. M., Electrical and Dielectric Properties of Stitched Non-woven Engineered Fabrics Containing Activated Carbon Fiber, *Egypt. J. Chem.* **61**, 559 - 568 (2018).

26. Steichen M., Djemour R., Gütay L., Guillot J., Siebentritt S., and Dale J. P., Direct Synthesis of

Single-Phase p-Type SnS by Electrodeposition from a Dicyanamide Ionic Liquid at High Temperature for Thin Film Solar Cells, *J. Phys. Chem. C*, **117**, 4383–4393(2013).

27. Nwofe P. A., Reddy K. T. R., and Miles R. W., Type conversion of p-SnS to n-SnS using a SnCl₄/ CH₃OH heat treatment, *IEEE 39th Photovoltaic Specialists Conference* (PVSC) (2013)**.**

28. Patel T. H., Low Temperature Chemical Synthesis of p-Type SnS Thin Films Suitable for Photovoltaic Structures, *Solid State Phenomena*, **209**, 82-85(2013).

29. Dillon R.O., Spain I. L., and McClure J.W., Electronic energy band parameters of graphite and their dependence on pressure, temperature and acceptor concentration, *J. Phy. & Chem. of Solids*, **38**, 635-645 (1977).

<div dir="rtl">

تأثير السلائف وأساليب التكوين على الخصائص البصرية والكهروكيميائيه الضوئية لطبقة امتصاص SnS

عاطف يوسف شنودة¹ و مصطفي محمد سند¹ و أوفيليا كوستادينوفا²

¹مركز بحوث و تطوير الفلزات- التبين – ص. ب. ٨٧ حلوان – مصر.
²معهد الكيمياء الكهربية و أنظمة الطاقة – أكاديمية العلوم البلغارية – ١١١٣ صوفيا – بلغاريا.

يعتبر تأثير طريقة الأعداد والسلائف المختلفة لامتصاص معاملات طبقة الأمتصاص للخلية الجهدية الضوئية. تم تكوين مركبات كبريتيد القصدير بكلا من طريقتي تفاعل الحالة الصلبة و الحرارية المائية باستخدام سلائف الكبريت المختلفة. وأجرت دراسة مورفولوجية علي الحبيبات و التعرف علي الصنف باستخدام تقنيات حيود الأشعة السينية (XRD) ومجهر حقل الانبعاث الماسح الإلكتروني. كشف نمط حيود XRD عن وجود بنية بلورية لصنفين: الغالبية أورثورومبيك و الأقلية رباعي. وحددت الخصائص البصرية باستخدام جهاز المطياف الضوئي ذو الأشعة المرئية- فوق البنفسجية والمرئية مظهرا قمم امتصاص عند حوالي ٤٨٥ نانومتر. أيضا كانت أدني طاقة فجوة مقدارها ١٫٧٤ الكترون- فولت لعينة كبريتيد قصدير محضر من مادة L-Cystine. كشفت قياسات المعاوقة الكهروكيميائية أن خلية كبريتيد القصدير المحضرة من L-Cystine أعطت أقل مقاومة ١٧١ أوم. أظهرت الخلية الضوئية الكهروكيميائية المحضرة من هذا المركب أعلى كفاءة تحويل الطاقة علي وحدة المساحة بمقدار ٢٫٥ في المائة.

</div>